Research Article Vol. 30, No. 8 / 11 Apr 2022 / Optics Express 13839
Optics EXPRESS

Emission bandwidth control on a two-dimensional superlattice microcavity array

ZHEN LIU,[1,2] MAKOTO SHIMIZU,[1,3] AND HIROO YUGAMI[1]

[1]Department of Mechanical Systems Engineering, Tohoku University, Sendai 980-8579, Japan
[2]liu.zhen.p5@dc.tohoku.ac.jp
[3]makoto.shimizu.a3@tohoku.ac.jp

Abstract: Narrowband thermal emission at high temperatures is required for various thermal energy systems. However, the large lossy energy of refractory metals induces a broad bandwidth emission. Here, we demonstrated a two-dimensional (2D) superlattice microcavity array on refractory metals to control the emission bandwidth. A hybrid resonance mode was obtained by coupling the standing-wave modes and propagating surface-wave modes. The bandwidth emission was controlled by varying the superlattice microcavity array resulting from the change in electric field (E-field) concentration. The quality factor (Q-factor) improved by more than 3 times compared to that of a single-lattice array. A narrower band emission originating from the hybrid mode was observed and analyzed experimentally. This novel surface-relief microstructure method can be used to control the emission bandwidth of thermal emitters used in thermophotovoltaic (TPV) systems and other high-temperature thermal energy systems.

1. Introduction

Controllable spectral properties are attractive for substantial applications in heat transfer [1–4], optoelectronics [5–7], and sensing technologies [8,9]. Spectral-controlled thermal emitters, which are expected to improve the efficiency of energy systems, have been extensively studied over the past century. The photonic structure is an appealing strategy because its spectral distribution can be flexibly adjusted over a wide wavelength range. Many researchers have demonstrated the spectral control of emissions with photonic microstructures (e.g., one-dimensional photonic multilayers [10–12], surface microstructures [13–17] and metamaterials [18–22]). Furthermore, the thermal stability of emitters is critical for high-temperature operations of energy conversion systems, such as TPV systems [23–27] and solar thermal systems [28–32]. Refractory metals (e.g., tantalum (Ta), tungsten, and molybdenum) are often used as thermal emitters owing to the high melting point characteristics. Several studies have reported the fabrication of photonic structures on these refractory metals [33,34]. Emission spectra are controlled by the interaction between the periodic lattice of microstructures and electromagnetic(EM) waves from high-temperature thermal sources. This concept is expected to improve the efficiency of energy systems.

Quasi-monochromatic thermal emissions have been demonstrated to significantly improve the efficiency of energy conversion systems. Several researchers have demonstrated various narrowband thermal emitters based on multiple quantum wells with photonic crystals (PhCs) [35], 2D periodic microcavities covered with a thin metal [36], and plasmonic Fano resonance in PhCs [37]. However, photonic microcavities formed by refractory metals are likely to be lossy in the near-infrared range, and the amplification of standing-wave modes is not sufficient to obtain a narrowband emission [38]. Controlling the bandwidth on the refractory metals for high-temperature thermal systems remains challenging. Owing to the flexibility of photonic microstructures, the manipulation of various resonances to induce coupling at desirable wavelengths has been demonstrated as an effective approach to control the spectrum properties. For example, the Fabry-Pérot (FP) mode was enhanced by coupling the plasmon resonance modes in a dielectric cavity [39]. A strong absorptance was observed upon coupling the magnetic

#455722 https://doi.org/10.1364/OE.455722
Journal © 2022 Received 7 Feb 2022; revised 30 Mar 2022; accepted 31 Mar 2022; published 8 Apr 2022

Optics EXPRESS

polaritons of a metal grating with the plasmonic resonance of a graphene ribbon [40]. Therefore, controlling the bandwidth in refractory metals by generating the hybrid resonance mode is an effective strategy.

In this study, we developed a 2D superlattice microcavity array to achieve bandwidth control of thermal emission using refractory metals. The standing-wave modes, which are regarded as microcavity resonances (MCR), are generated in individual microcavities, and the propagating surface-wave modes, which are regarded as surface plasmon resonances (SPR), are generated at the surface of the periodic microcavity array. The hybrid resonance mode appears by tuning the resonance wavelengths of the MCR and SPR. Here, a strong enhancement of the localized E-field distribution was obtained by controlling the gap between adjacent microcavities. The emission bandwidth was proven to be controllable experimentally. This novel strategy demonstrated that the emission bandwidth from refractory metals can be controlled by the 2D superlattice microcavity array. This reduces the complexity of fabrication, making it convenient to use arbitrary refractory metals as large-area thermal emitters, which are used in thermophotovoltaic systems and other high-temperature thermal energy systems.

2. Design and fabrication

2.1. Hybrid resonance mode generation

The proposed 2D superlattice structure consists of a pair of square cavities with diverse aperture sizes and is distributed in an anti-symmetry crossing (see Fig. 1(a) and (b)). The large cavity, hereinafter referred to as the main cavity, acts as the resonator of the MCR and confines the EM wave. The smaller cavity is referred to as the supplementary cavity. The superlattice periodic array was constructed using both microcavities to generate the SPR. The resonant wavelengths of the MCR and SPR can be expressed by Eqs. (1) [41] and (2) [42], respectively.

$$\lambda_{peak,MCR} = \frac{2}{\sqrt{\left(\frac{l}{L_x}\right)^2 + \left(\frac{m}{L_y}\right)^2 + \left(\frac{2n+1}{2L_z}\right)^2}} \tag{1}$$

$$\lambda_{peak,SPR} = \frac{\Lambda}{m}\left(1 \pm \sin\theta\cos\phi\right)\sqrt{\frac{\varepsilon_m}{1+\varepsilon_m}} \tag{2}$$

where l, m, and n are integers, L_x, L_y are the aperture width values of the microcavity, and L_z is the microcavity depth. Λ is the grating period, θ and ϕ are the polar and azimuthal angles, respectively, and ε_m is the dielectric constant of the metal.

The excitation of hybrid resonance mode was designed at ~1.7 μm to demonstrate the effectiveness of bandwidth control in the near-infrared range. Moreover, the normal incident light was considered as the surface propagation waves to couple with the metallic periodic grating for SPR generation. Therefore, we coupled the MCR and SPR to generate the hybrid resonance mode at small wave vectors by optimizing the geometrical structure. The following parameters were used for the Ta substrate: a period λ of 1.1 μm, main cavity width a_1 of 0.9 μm, supplementary cavity width a_2 of 0.7 μm, and an etch depth d of 0.7 μm. The dispersion curve of the hybrid resonance mode is shown in Fig. 1(c). A clear resonance coupling behavior was observed near the wave vectors $K_x = 0$, where the interaction between the standing waves of the MCR at the upper branch and the propagation waves of the SPR at the lower branch. Compared to the independent excitation of MCR and SPR at the large wave vectors. We note that the intensity of the emission spectra was strongly enhanced in the resonance coupling range. It indicates that a large part of the thermal energy would emit from the hybrid resonance mode.

Optics EXPRESS

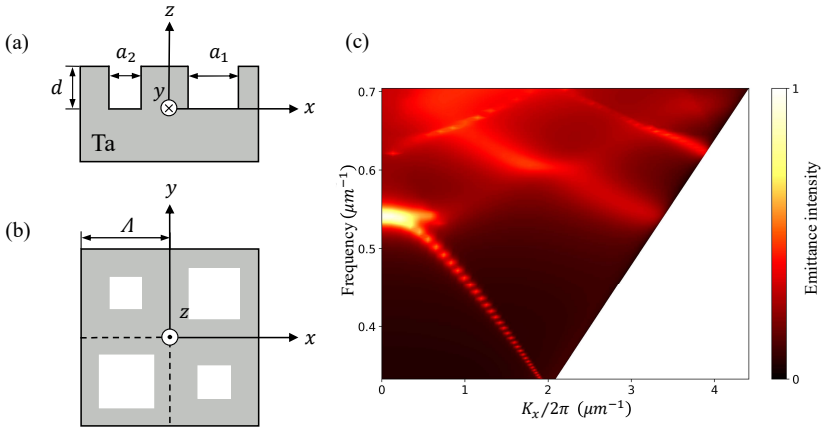

Fig. 1. (a) Schematic illustration of the 2D superlattice microcavity array on Ta substrate in cross-section view. (b) Top view; all key geometrical parameters are indicated. (c) Calculated dispersion curve of hybrid resonance mode in the 2D superlattice microcavity array.

2.2. *Emission bandwidth control by supplementary cavity*

According to Eqs. (1) and (2), hybrid coupling can be generated regardless of the geometrical features of the supplementary cavity. To investigate the spectral dependence of the hybrid resonance mode in various supplementary cavity sizes, the spectral emittance was simulated with a_2=0, 0.4, 0.7, 0.8, and 0.9 μm (see Fig. 2). The simulations used a rigorous coupled-wave analysis (RCWA) method at the wave vector $K_x = 0$ and both s- and p-polarized. When $a_2 = 0$, the emission peak was observed at $\lambda = 1.79$ μm, which was attributed to the hybrid resonance mode excitation in the 2D superlattice microcavity array. The spectral properties for the $a_2 = 0.4$ μm case were similar to those of $a_2 = 0$. A narrowing of the emission band was clearly observed in the $a_2 = 0.7$ μm case. Subsequently, the emission peak rapidly degraded in the $a_2 = 0.8$ μm, where in the supplementary cavity size approaches the main cavity size. A broad peak was observed in the $a_2 = 0.9$ μm. We postulated that the peak appearing at $\lambda = 1.69$ μm could be attributed to pure MCR.

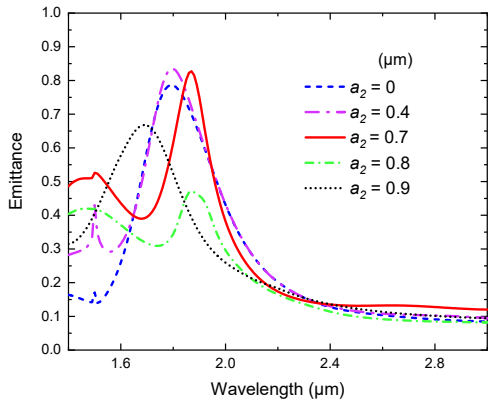

Fig. 2. Calculated spectral emittance for the superlattice microcavity array structure at wave vector $K_x = 0$ with $\Lambda = 1.1$ μm, $a_1 = 0.9$ μm, $d = 0.7$ μm and $a_2 = 0$, 0.4, 0.7, 0.8, and 0.9 μm.

Optics EXPRESS

To elucidate the controlling mechanism of the supplementary cavity structure on the emission bandwidth, E-field amplitudes at the resonance wavelength were calculated. Here, E_z denotes the amplitude at the grating surface and E_x denotes the microcavity center. The E-field distributions at a_2 = 0, 0.4 μm, 0.7 μ, and 0.9 μm superimposed with the corresponding 2D superlattice microcavity array structure are shown in Figs. 3. We note that the E-field distribution of E_z was localized on the gap surface between the adjacent main cavity and the supplementary cavity, which is consistent with the SPR excitation in the superlattice microcavity array. The intensity of the E-field between adjacent cavities was enhanced when the supplementary cavity size increased. This can be attributed to the density enhancement of the plasmon oscillation on the periodic grating, because the gap between the adjacent cavities was compressed. Hence, the SPR excitation was enhanced by the E-field concentration effect. The MCR excitation was demonstrated by the E-field about E_x, where the standing waves were confined to the main cavity.

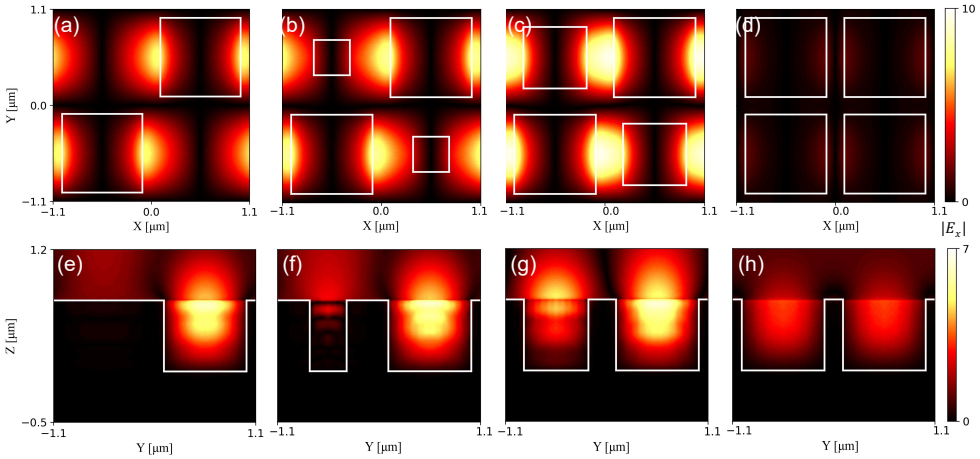

Fig. 3. (a–d) Calculated E-field distribution of E_z for the surface propagation waves at *xoy*-cut plane where z = 0.8 μm. (e–h) Calculated E-field distribution of E_x for the cavity standing waves at *yoz*-cut plane where x = 0.55 μm.

The dependence of the E-field amplitude on the supplementary cavity size was investigated at each emission peak (see Fig. 4). E_z indicates the intensity of surface waves propagation by SPR excitation, and E_x indicates the intensity of standing waves formed in the cavity. E_z increased rapidly after a_2>0.4 μm, and the maximum value was obtained with a_2 = 0.7 μm; a similar trend was observed for E_x. The E-field distribution was converted to the profile of the single-lattice array when $a_1 = a_2$, which indicates that the hybrid resonance mode was changed to the pure MCR mode. This resonance mode change caused the degradation of E_x and E_z. These analyses show that the bandwidth variation can be attributed to the localized enhancement of the E-field in the hybrid resonance mode, which was achieved by varying the size of the supplementary cavity.

2.3. Fabrication

The 2D superlattice microcavity array fabrication process for polished Ta substrate is similar to a developed process for photonic microstructures fabrication [43]. A 30 *nm* layer of chromium (Cr), followed by a 180 *nm* layer of silicon dioxide (SiO_2) were deposited by radio frequency magnetron sputtering onto the cleaned substrates. These layers worked as the hard mask for the Ta etching. The 2D superlattice microcavity array was defined on a 400 *nm*-thick soft resist (ZEP-520A) by electron beam (EB) lithography. After the resist development, the pattern was transferred into the SiO_2 and Cr mask layers by trifluoromethane (CHF_3) and chlorine (Cl_2)/oxygen (O_2) with

Optics EXPRESS

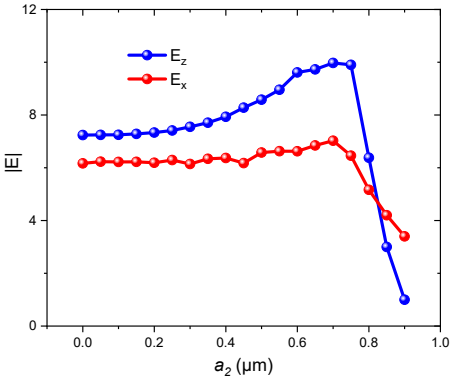

Fig. 4. Dependence of E-field intensity E_z and E_x at emission peak on various aperture sizes of the supplementary cavity.

induced coupled plasma reactive ion etching (ICP-RIE), respectively, using ULVAC CE-300I. The Ta substrate was finally etched by dry etching using sulfur hexafluoride (SF_6) to form the cavities. The residual Cr layer was removed completely by immersion into Cr liquid etchant (MicroChemicals).

3. Results and discussion

Three samples were fabricated with the following supplementary cavity sizes: $a_2 = 0$, 0.4, and 0.7 μm. The following geometrical structure parameters were fixed: $\Lambda = 1.1$ μm, $a_1 = 0.9$ μm, and $d = 0.7$ μm. To characterize the spectral emittance of the fabricated samples, the reflectance was measured at room temperature from 1.5 μm to 3 μm using FT-IR (Spectrum-6100, JASCO) with an indium antimonide (InSb) photodiode detector. The non-polarized incident light parameters used for the measurement were $\theta = 10^\circ$ and $\phi = 45^\circ$. Because the samples were opaque, the emittance was derived from the measured reflectance: $A(\lambda) = 1 - R(\lambda)$. The measured and simulated emittance values are shown in Figs. 5(a)–(c); the respective scanning electron microscopy (SEM) images are shown in the inset. According to the simulation results, the disturbance in the diffraction reflection only affects the measured spectrum for wavelengths wavelength shorter than 1.78 μm. Therefore, the diffraction effect did not occur in the hybrid resonance peak at 1.81, 1.9, and 1.97 μm with $a_2 = 0$, 0.4, and 0.7 μm, respectively. This means that it is possible to evaluate the emittance from the measured normal reflectance in this range. The measured spectrum of the hybrid resonance peak showed good agreement with the simulated spectrum. The bandwidth became narrower when the supplementary cavity was enlarged by the E-field concentration effect. The slightly broader bandwidth of the measured peak can be explained by the surface roughness of the cavity sidewall in the RIE process.

The Q-factor was obtained by fitting the hybrid resonance peak using the Voigt function. As described in the analysis, the Q-factor is a function of the supplementary cavity size, which is attributed to the E-field concentration effect. A narrowband emission with a Q-factor of 12.4 was obtained at $a_2 = 0.7$ μm in the 2D superlattice microcavity array, compared with a Q-factor of 4.1 in the single-lattice array. The experimentally resultant spectrum confirmed the improvement of the Q-factor obtained by compressing the gap between adjacent microcavities. (see Fig. 5(d)). These results demonstrate that the emission bandwidth can be controlled by the size of the supplementary cavity with the hybrid resonance mode in a 2D superlattice microcavity array. Moreover, several studies have demonstrated that the desired spectral performance of the surface grating microstructure can be realized in a high-temperature environment [44–45]. Furthermore, several effective approaches were reported to improve thermal stability [46,47]. For example, a

Optics EXPRESS

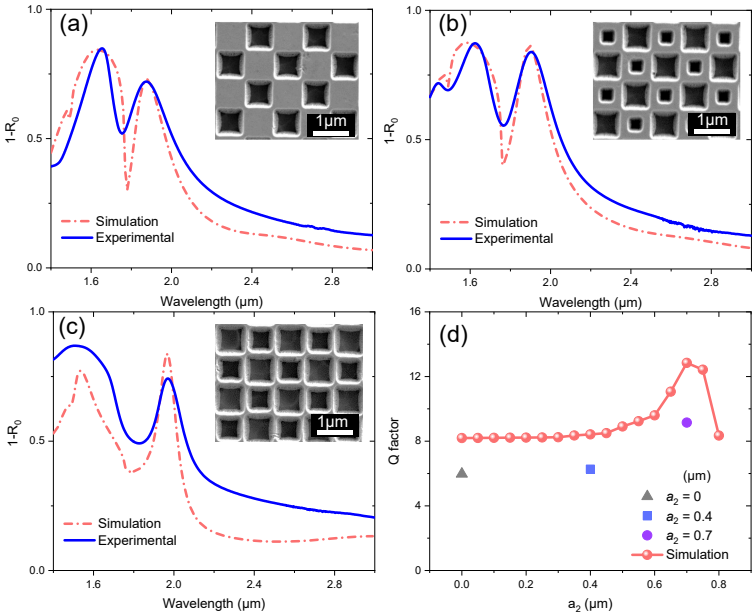

Fig. 5. (a–c) Measured and simulated emittances for 2D superlattice microcavity array. The structural parameters are $\Lambda = 1.1\ \mu m$, $a_1 = 0.9\ \mu m$, and $d = 0.7\ \mu m$ with $a_2 = 0$, 0.4, and $0.7\ \mu m$, respectively. Insets show the SEM images of fabricated samples. (d) Q-factor of the hybrid resonance mode peak as a function of the supplementary cavity size.

protective barrier was induced by coating a thin conformal layer of hafnia for long operational lifetimes. Therefore, owing to the similar structural characteristics with the 2D surface grating and flexible design that can integrate with various methods. The 2D superlattice microcavity array demonstrates the significant potential to realize the satisfactory robustness of the thermal stability and spectral emittance at high temperatures.

4. Conclusions

In summary, a 2D superlattice array was proposed for surface-relief microcavities on refractory metals to realize emission bandwidth control for thermal energy systems. We demonstrated hybrid resonance excitation by bonding the resonance of MCR and SPR. The spectrum of hybrid resonance mode strongly depends on the aperture size of the supplementary cavity, which plays a role in controlling the E-field concentration effect. A strong interaction of the E-field between the superlattice cavities was observed at $a_2 = 0.7\ \mu m$, indicating that the large supplementary cavity enhances the plasmon oscillation on the surface of the metal grating. Thus, the emission bandwidth of the hybrid resonance mode can be controlled by embedding various supplementary cavities. A narrower emission bandwidth was observed with the superlattice microcavity array, and the Q-factor of the emission peak improved by 3 times compared to that of the single-lattice array. The improvement of the Q-factor was experimentally confirmed. The 2D superlattice microcavity array provides a novel strategy for realizing quasi-monochromatic thermal radiation with an integrated structured emitter or thermophotovoltaic systems and other high-temperature thermal energy systems.

Funding. Japan Society for the Promotion of Science (KAKENHI Grant Number JP21K04894).

Acknowledgments. We would like to thank Mr. M. Hemmi and Mr. T. Kikuta for instruction in the fabrication. Part of this work was supported by the Graduate Program for Integration of Mechanical Systems, Tohoku University. The

Optics EXPRESS

facility used in this study was partly supported by Nanotechnology Platform Project Sponsored By The Ministry Of Education, Culture, Sports, Science And Technology (MEXT), Japan.

Disclosures. The authors declare no conflicts of interest.

Data availability. Data underlying the results presented in this paper are not publicly available at this time but may be obtained from the authors upon reasonable request.

References

1. B. Zhao, K. Chen, S. Buddhiraju, G. Bhatt, M. Lipson, and S. Fan, "High-performance near-field thermophotovoltaics for waste heat recovery," Nano Energy **41**, 344–350 (2017).
2. M. Lim, J. Song, S. S. Lee, and B. J. Lee, "Tailoring near-field thermal radiation between metallo-dielectric multilayers using coupled surface plasmon polaritons," Nat. Commun. **9**(1), 1–9 (2018).
3. A. Leroy, B. Bhatia, C. C. Kelsall, A. Castillejo-Cuberos, M. H. Di Capua, L. Zhao, L. Zhang, A. M. Guzman, and E. N. Wang, "High-performance subambient radiative cooling enabled by optically selective and thermally insulating polyethylene aerogel," Sci. Adv. **5**(10), 1–9 (2019).
4. S. Fan and W. Li, "Photonics and thermodynamics concepts in radiative cooling," Nat. Photonics **16**(3), 182–190 (2022).
5. Z. Yang, M. Liu, S. Liang, W. Zhang, T. Mei, D. Zhang, and S. J. Chua, "Hybrid modes in plasmonic cavity array for enhanced hot-electron photodetection," Opt. Express **25**(17), 20268 (2017).
6. C. Zhang, Q. Huang, Q. Cui, C. Ji, Z. Zhang, X. Chen, T. George, S. Zhao, and L. J. Guo, "High-Performance Large-Scale Flexible Optoelectronics Using Ultrathin Silver Films with Tunable Properties," ACS Appl. Mater. Interfaces **11**(30), 27216–27225 (2019).
7. S. Hassan, C. F. Doiron, and G. V. Naik, "Optimum selective emitters for efficient thermophotovoltaic conversion," Appl. Phys. Lett. **116**(2), 023903 (2020).
8. R. Ameling, L. Langguth, M. Hentschel, M. Mesch, P. V. Braun, and H. Giessen, "Cavity-enhanced localized plasmon resonance sensing," Appl. Phys. Lett. **97**(25), 253116 (2010).
9. N. Karker, G. Dharmalingam, and M. A. Carpenter, "Thermal energy harvesting plasmonic based chemical sensors," ACS Nano **8**(10), 10953–10962 (2014).
10. P. N. Dyachenko, S. Molesky, A. Y. Petrov, M. Störmer, T. Krekeler, S. Lang, M. Ritter, Z. Jacob, and M. Eich, "Controlling thermal emission with refractory epsilon-near-zero metamaterials via topological transitions," Nat. Commun. **7**(1), 11809 (2016).
11. W. Li, Y. Shi, Z. Chen, and S. Fan, "Photonic thermal management of coloured objects," Nat. Commun. **9**(1), 4240 (2018).
12. X. Liu, Z. Li, Z. Wen, M. Wu, J. Lu, X. Chen, X. Zhao, T. Wang, R. Ji, Y. Zhang, L. Sun, B. Zhang, H. Xu, J. Zhou, J. Hao, S. Wang, X. Chen, N. Dai, W. Lu, and X. Shen, "Large-area, lithography-free, narrow-band and highly directional thermal emitter," Nanoscale **11**(42), 19742–19750 (2019).
13. Y. B. Chen and Z. M. Zhang, "Design of tungsten complex gratings for thermophotovoltaic radiators," Opt. Commun. **269**(2), 411–417 (2007).
14. M. Shimizu, K. Konno, F. Iguchi, and H. Yugami, "Fabrication of quasi-periodic surface microcavities by selective etching of self-organized superalloys for high-temperature photonics," Appl. Phys. Lett. **101**(22), 221901 (2012).
15. Y. X. Yeng, M. Ghebrebrhan, P. Bermel, W. R. Chan, J. D. Joannopoulos, M. Soljačić, and I. Celanovic, "Enabling high-temperature nanophotonics for energy applications," Proc. Natl. Acad. Sci. U. S. A. **109**(7), 2280–2285 (2012).
16. D. Woolf, J. Hensley, J. G. Cederberg, D. T. Bethke, A. D. Grine, and E. A. Shaner, "Heterogeneous metasurface for high temperature selective emission," Appl. Phys. Lett. **105**(8), 081110 (2014).
17. M. Shimizu, T. Yamada, K. Sasaki, A. Takada, H. Nomura, F. Iguchi, and H. Yugami, "Anisotropic multi-step etching for large-area fabrication of surface microstructures on stainless steel to control thermal radiation," Sci. Technol. Adv. Mater. **16**(2), 025001 (2015).
18. N. Mattiucci, G. D'Aguanno, A. Alù, C. Argyropoulos, J. V. Foreman, and M. J. Bloemer, "Taming the thermal emissivity of metals: A metamaterial approach," Appl. Phys. Lett. **100**(20), 201109 (2012).
19. B. Zhao and Z. M. Zhang, "Study of magnetic polaritons in deep gratings for thermal emission control," J. Quant. Spectrosc. Radiat. Transfer **135**, 81–89 (2014).
20. W. Gu, G. Tang, and W. Tao, "High efficiency thermophotovoltaic emitter by metamaterial-based nano-pyramid array," Opt. Express **23**(24), 30681 (2015).
21. C. Guo, Y. Guo, B. Lou, and S. Fan, "Wide wavelength-tunable narrow-band thermal radiation from moiré patterns," Appl. Phys. Lett. **118**(13), 131111 (2021).
22. D. Lee, S. So, G. Hu, M. Kim, T. Badloe, H. Cho, J. Kim, H. Kim, C.-W. Qiu, and J. Rho, "Hyperbolic metamaterials: fusing artificial structures to natural 2D materials," eLight **2**(1), 1 (2022).
23. A. Lenert, D. M. Bierman, Y. Nam, W. R. Chan, I. Celanović, M. Soljačić, and E. N. Wang, "A nanophotonic solar thermophotovoltaic device," Nat. Nanotechnol. **9**(2), 126–130 (2014).
24. A. Kohiyama, M. Shimizu, H. Kobayashi, F. Iguchi, and H. Yugami, "Spectrally Controlled Thermal Radiation Based on Surface Microstructures for High-Efficiency Solar Thermophotovoltaic system," Energy Procedia **57**, 517–523 (2014).

Optics EXPRESS

25. K. Chen, P. Santhanam, and S. Fan, "Suppressing sub-bandgap phonon-polariton heat transfer in near-field thermophotovoltaic devices for waste heat recovery," Appl. Phys. Lett. **107**(9), 091106 (2015).
26. A. Kohiyama, M. Shimizu, and H. Yugami, "Unidirectional radiative heat transfer with a spectrally selective planar absorber/emitter for high-efficiency solar thermophotovoltaic systems," Appl. Phys. Express **9**(11), 112302 (2016).
27. A. Kohiyama, M. Shimizu, K. Konno, T. Furuhashi, and H. Yugami, "Effective photon recycling in solar thermophotovoltaics using a confined cuboid emitter," Opt. Express **28**(26), 38567 (2020).
28. D. Chester, P. Bermel, J. D. Joannopoulos, M. Soljacic, and I. Celanovic, "Design and global optimization of high-efficiency solar thermal systems with tungsten cermets," Opt. Express **19**(S3), A245 (2011).
29. C. Shemelya, D. Demeo, N. P. Latham, X. Wu, C. Bingham, W. Padilla, and T. E. Vandervelde, "Stable high temperature metamaterial emitters for thermophotovoltaic applications," Appl. Phys. Lett. **104**(20), 201113 (2014).
30. H. Wang, V. Prasad Sivan, A. Mitchell, G. Rosengarten, P. Phelan, and L. Wang, "Highly efficient selective metamaterial absorber for high-temperature solar thermal energy harvesting," Sol. Energy Mater. Sol. Cells **137**, 235–242 (2015).
31. M. Shimizu, H. Akutsu, S. Tsuda, F. Iguchi, and H. Yugami, "A high-temperature solar selective absorber based upon periodic shallow microstructures coated by multi-layers using atomic layer deposition," Photonics **3**(2), 13 (2016).
32. M. Shimizu, Z. Liu, and H. Yugami, "Amorphous Nanohole Patterns Formed by Spinodal Decomposition of Nickel Superalloys for Solar-Selective Absorbers," ACS Appl. Nano Mater. **3**(9), 9502–9509 (2020).
33. H. Sai and H. Yugami, "Thermophotovoltaic generation with selective radiators based on tungsten surface gratings," Appl. Phys. Lett. **85**(16), 3399–3401 (2004).
34. V. Stelmakh, V. Rinnerbauer, R. D. Geil, P. R. Aimone, J. J. Senkevich, J. D. Joannopoulos, M. Soljačić, and I. Celanovic, "High-temperature tantalum tungsten alloy photonic crystals: Stability, optical properties, and fabrication," Appl. Phys. Lett. **103**(12), 123903 (2013).
35. M. De Zoysa, T. Asano, K. Mochizuki, A. Oskooi, T. Inoue, and S. Noda, "Conversion of broadband to narrowband thermal emission through energy recycling," Nat. Photonics **6**(8), 535–539 (2012).
36. A. Kohiyama, M. Shimizu, F. Iguchi, and H. Yugami, "Narrowband thermal radiation from closed-end microcavities," J. Appl. Phys. **118**(13), 133102 (2015).
37. C. Bauer and H. Giessen, "Tailoring the plasmonic Fano resonance in metallic photonic crystals," Nanophotonics **9**(2), 523–531 (2020).
38. Z. Liu, M. Shimizu, and H. Yugami, "Quantitative evaluation of optical properties for defective 2D metamaterials based on diffraction imaging," Opt. Express **28**(4), 5812 (2020).
39. T. Abhilash, M. Balasubrahmaniyam, A. Patra, and S. Kasiviswanathan, "Plasmon resonance mediated enhancement in Fabry-Pérot cavity modes," Appl. Phys. Lett. **104**(24), 241112 (2014).
40. B. Zhao and Z. M. Zhang, "Strong Plasmonic Coupling between Graphene Ribbon Array and Metal Gratings," ACS Photonics **2**(11), 1611–1618 (2015).
41. S. Maruyama, T. Kashiwa, H. Yugami, and M. Esashi, "Thermal radiation from two-dimensionally confined modes in microcavities," Appl. Phys. Lett. **79**(9), 1393–1395 (2001).
42. A. Heinzel, V. Boerner, A. Gombert, B. Bläsi, V. Wittwer, and J. Luther, "Radiation filters and emitters for the NIR based on periodically structured metal surfaces," J. Mod. Opt. **47**(13), 2399–2419 (2000).
43. V. Rinnerbauer, S. Ndao, Y. Xiang Yeng, J. J. Senkevich, K. F. Jensen, J. D. Joannopoulos, M. Soljačić, I. Celanovic, and R. D. Geil, "Large-area fabrication of high aspect ratio tantalum photonic crystals for high-temperature selective emitters," J. Vac. Sci. Technol., B: Nanotechnol. Microelectron.: Mater., Process., Meas., Phenom. **31**(1), 011802 (2013).
44. H. Sai, Y. Kanamori, and H. Yugami, "High-temperature resistive surface grating for spectral control of thermal radiation," Appl. Phys. Lett. **82**(11), 1685–1687 (2003).
45. V. Rinnerbauer, A. Lenert, D. M. Bierman, Y. X. Yeng, W. R. Chan, R. D. Geil, J. J. Senkevich, J. D. Joannopoulos, E. N. Wang, M. Soljačić, and I. Celanovic, "Metallic photonic crystal absorber-emitter for efficient spectral control in high-temperature solar thermophotovoltaics," Adv. Energy Mater. **4**(12), 1400334 (2014).
46. K. A. Arpin, M. D. Losego, A. N. Cloud, H. Ning, J. Mallek, N. P. Sergeant, L. Zhu, Z. Yu, B. Kalanyan, G. N. Parsons, G. S. Girolami, J. R. Abelson, S. Fan, and P. V. Braun, "Three-dimensional self-assembled photonic crystals with high temperature stability for thermal emission modification," Nat. Commun. **4**(1), 2630 (2013).
47. V. Stelmakh, W. R. Chan, M. Ghebrebrhan, J. Senkevich, J. D. Joannopoulos, M. Soljacic, and I. Celanovic, "Sputtered Tantalum Photonic Crystal Coatings for High-Temperature Energy Conversion Applications," IEEE Trans. Nanotechnology **15**(2), 303–309 (2016).